Nanopatterned $L1_0$-FePt Nanoparticles from Single Source of Metallopolymeric Precursors for Ferromagnetic Bit Patterned Media Magnetic Recording

Zhengong Meng,[a] Guijun Li,[b] Sheung-Mei Ng,[b] Hon-Fai Wong,[b] Sze-Chun Yiu,[a]

Cheuk-Lam Ho*,[a,c] Chi-Wah Leung*, [b] Wai-Yeung Wong*[a,c]

[a] *Institute of Molecular Functional Materials, Department of Chemistry, Partner State Key Laboratory of Environmental and Biological Analysis and Institute of Advanced Materials, Hong Kong Baptist University, Waterloo Road, Kowloon Tong, Hong Kong, P. R. China.*
E-mail: rwywong@hkbu.edu.hk; clamho@hkbu.edu.hk; Fax: +852-3411-7348
[b] *Department of Applied Physics, Hong Kong Polytechnic University, Hung Hom, Hong Kong, P. R. China.*
E-mail: dennis.leung@polyu.edu.hk
[c] *HKBU Institute of Research and Continuing Education, Shenzhen Virtual University Park, Shenzhen, 518057, P. R. China.*

Abstract

Bit patterned media (BPM) with precise stoichiometry ratio of FePt atoms is great promising for future high areal density magnetic recording. Herein, we report a new FePt-containing metallopolymer **P** as the single source for metal alloy nanoparticles synthesis. This polymer was synthesized from random copolymer poly(styrene-4-ethynylstyrene) **PES-PS** functionalized with bimetallic precursor **TPy-FePt** ([Pt(4'-ferrocenyl-(N^N^N))Cl]Cl) by Sonogarshira coupling reaction. After pyrolysis of **P**, the stoichiometry of Fe and Pt atoms in the synthesized nanoparticles (NPs) is nearly close to 1:1, which is more precise than using **Py-FePt** as precursor. Polymer **P** was also more favorable for patterning by high throughout nanoimprint lithography (NIL) as compared to **TPy-FePt**. Ferromagnetic nanolines, potentially as bit patterned media magnetic recording media, were successfully fabricated from **P** and have been fully characterized.

Introduction

Bimetallic nanoparticles (NPs) have been comprehensively studied recently, thanks to their unique properties from the synergistic effects of the individual metals.[1-4] Among these functional NPs, the $L1_0$ phase FePt NPs is one of the most vital materials with widely applications ranging from next generation ultrahigh-density magnetic recording media[5-7] to highly enhanced electrocatalysis.[8,9] This chemically ordered face centered tetragonal (fct) structure of FePt exhibits large uniaxial magnetocrystalline anisotropy (K_u) of 7×10^6 J/m^3, due to its spin-orbit coupling and the hybridization between Fe 3d and Pt 5d states.[10]

Chemical reduction[11,12] and polyol process[13-15] are the most well-established chemical methods for producing these fct phase FePt NPs.[16,17] Chemical disordered face-centered cubic (fcc) phase FePt NPs could be synthesized by these two routes, and they were further transformed to fct phase after high temperature annealing. However, agglomerations of the annealed NPs were frequently observed, yielding unfavorable shapes and size distributions of the resulting NPs.[13, 18] In addition, it is challenging for alloy nucleus growth from two individual sources with different reaction temperatures.[19] Thus, there is urgent need to chemically prepare FePt NPs from single-source precusors.

Recently, single source bimetallic carbonyl clusters have been intensively studied, such as $(CO)_3Fe(\mu\text{-dppm})(\mu\text{-CO})PtCl_2$,[20,21] $FePt(CO)_4dppmBr_2$[22] and polycrystalline $FePtCl_6$,[23] etc. The atomic ratios of Fe and Pt were precisely sustained from these single source precursors, owing to the close integration of Fe and Pt atoms

during the nucleation process. However, the FePt NPs synthesized from these routes are difficult to form the required nanopatterns on thin film for bit patterned magnetic recording media.

An alternative approach for producing $L1_0$ phase FePt NPs was by the one-step pyrolysis of ferroplatinyne polymer. Through fine tuning the Fe and Pt atomic ratio in the organic framework at molecular dimensions, our group has successfully synthesized FePt NPs with high magnetic coercivities after pyrolysis under inert atmosphere. [24-26] The residual carbon after pyrolysis effectively isolates the individual FePt NPs, inhibiting the agglomerations during high temperature processes. However, the molecular weights of these polymers were relative large, because the metallic atoms are embedded in the main chains of the polymers.

With emerging demand for higher recording density for data storage device, the current perpendicular magnetic recording architecture cannot satisfy the requirement for areal density over 1 T/in^2. The main challenge is the significant data loss after further increasing the recording bit density, due to the unstable magnetic direction of individual bit caused by the thermal fluctuations of the adjacent recording bits. Although fct phase FePt NPs have ultrahigh anisotropy at room tempature, it is still challenging to achive reliable storage after the bit size squeeze down below 10 nm.[11] Thus, the bit patterned media architecture was proposed to solve the thermal instability challenge. By sterically isolating the adjacent bit, the interaction of the nearest two bits can be significantly inhibited. Patterning of FePt NPs for magnetic recording have been investigated by thermal, self-assembly, and lithography

patterning.[27] However, these patterning methods suffered from either high-cost or short range ordering difficulties, which represent a challenge for practical hard disk drive productions. Meanwhile, the high throughout nanoimprint lithography (NIL) is an effective method for industrial grade nano patterning.[28, 29] With reusable imprint mold, the nano patterns can be replicated from mask to functional materials with resolution below 10 nm.[30, 31] Based on our previous studies of patterning of FePt NPs from main chain polymers,[26 25, 32] herein we report a novel single source metallic polymer **P** with functional bimetallic fragment on the side chains. The Fe and Pt stoichiometric ratio was accurately controlled in this polymer. This polymer **P** was successfully patterned by NIL, desired fct phase of FePt NPs was readily obtained directly after pyrolysis under inert gas atmosphere without the need of post-phase transformation. As compared to molecular **TPy-FePt** as the source for FePt NPs synthesis, more accurate control of the atomic ratios, narrower size distributions and stronger magnetic coercivity of NPs were synthesized by **P**.

Results and discussions

Ferrocene-functionalized terpyridine ligand was synthesized by the one-step approach modified from the literature report as shown in scheme 1.[33] After coordinated with Pt ion, the bimetallic complex **TPy-FePt** was synthesized. On the other hand, the random copolymer poly[(4-trimethylsilyl)ethylnylstyrene-styrene] (**PTMES-PS**) was synthesized via free radical polymerization. The **PES-PS** was produced after the deprotection of the TMS group on **PTMES-PS** by

tetrabutylammonium fluoride (TBAF). Then the bimetallic copolymer **P** was prepared from **PES-PS** by Sonogashira reaction with **TPy-FePt**. All the new metal complex, polymer precursors and polymer **P** are air-stable. Systematic characterization of these compounds was achieved by analytical and spectroscopic methods. The IR and NMR (^{1}H and ^{13}C) data are in accordance with their chemical structures. GPC analysis was used to estimate the molecular weight of **PTMES-PS**. The thermal property of new polymer **P** was examined by thermal gravimetric analysis (TGA) under nitrogen. Analysis of the TGA trace for the polymer shows that it has high onset decomposition temperature of 291 ^{o}C, indicative of its good thermal stability.

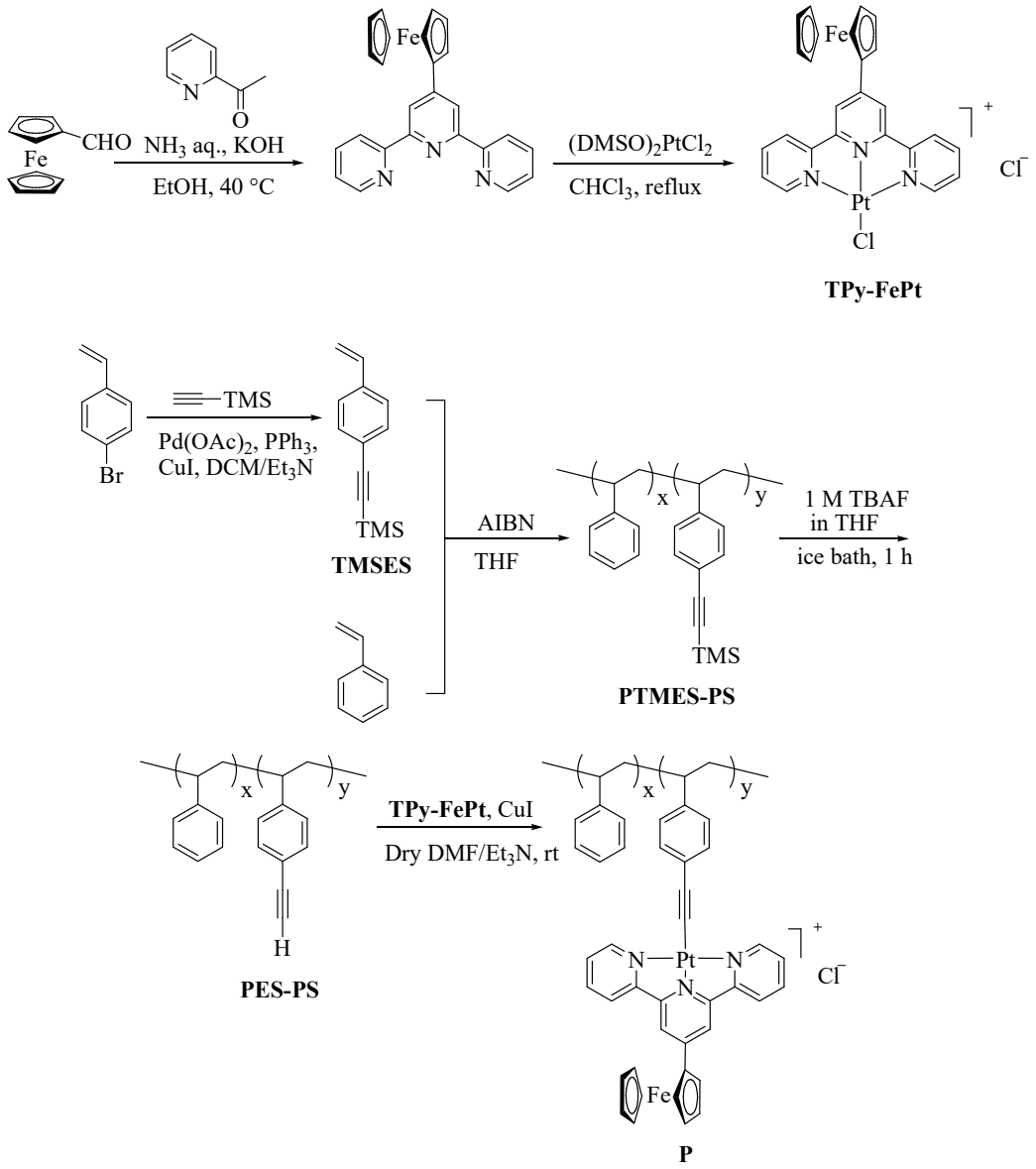

Scheme 1 Synthetic routes for bimetallic precursor **TPy-FePt** and copolymer **P**.

For comparing the properties of NPs generated from small molecule **TPy-FePt** and metallopolymer **P**, the two precursors were heated to 800 °C for 1 h separately in the same conditions. Heating rates of 10 °C min^{-1} under protective gas environments (95% Ar + 5% H_2) were used to synthesize NPs **FePt-1** and **FePt-2** from **TPy-FePt** and **P** accordingly. The nanostructures, size distributions, and the atomic elementary

composition of the resultant FePt NPs were then examined by TEM, as shown in Figures 1a–1c and 1d–1f, respectively, for **FePt-1** and **FePt-2**. As shown in Fig. 1a, **FePt-1** NPs are in square-like shapes within the amorphous carbonaceous matrix. The cube shape NPs[34] has obvious lattice fringe at 0.19 nm, which corresponding to the (200) plane of $FePt_3$ as shown in the high-resolution TEM image in Fig. 1b. The side length of **FePt-1** NPs behaves Gaussian shapes distribution with center at 6.9 nm (Fig. 1c). The atomic ratio of the Fe and Pt atoms is 30:70 according to the Energy Dispersive X-ray (EDX) spectrum, indicating the form of **FePt-1** NPs is mostly $FePt_3$. Meanwhile, the TEM result shows the **FePt-2** to be typical fct phase FePt. Spherical, rather than square shaped NPs are embedded in the carbon matrix as shown in Fig. 1d. Significant crystalline fringes with lattice distances of 0.229, 0.281, and 0.376 nm, according to fct phase (111), (110) and (001) planes, respectively, are shown in the high resolution TEM image of Fig. 1e. Larger mean size at ca. 7.4 nm is shown in the Gaussian shape distributions in Fig. 1f for **FePt-2**. The EDX results also indicate that close to the same atomic ratio of Fe and Pt atoms (48:52) was formed in **FePt-2**. The above TEM results show that **FePt-1** NPs generated from **TPy-FePt** is $FePt_3$ phase, while **FePt-2** obtained from **P** is fct phase FePt NPs.

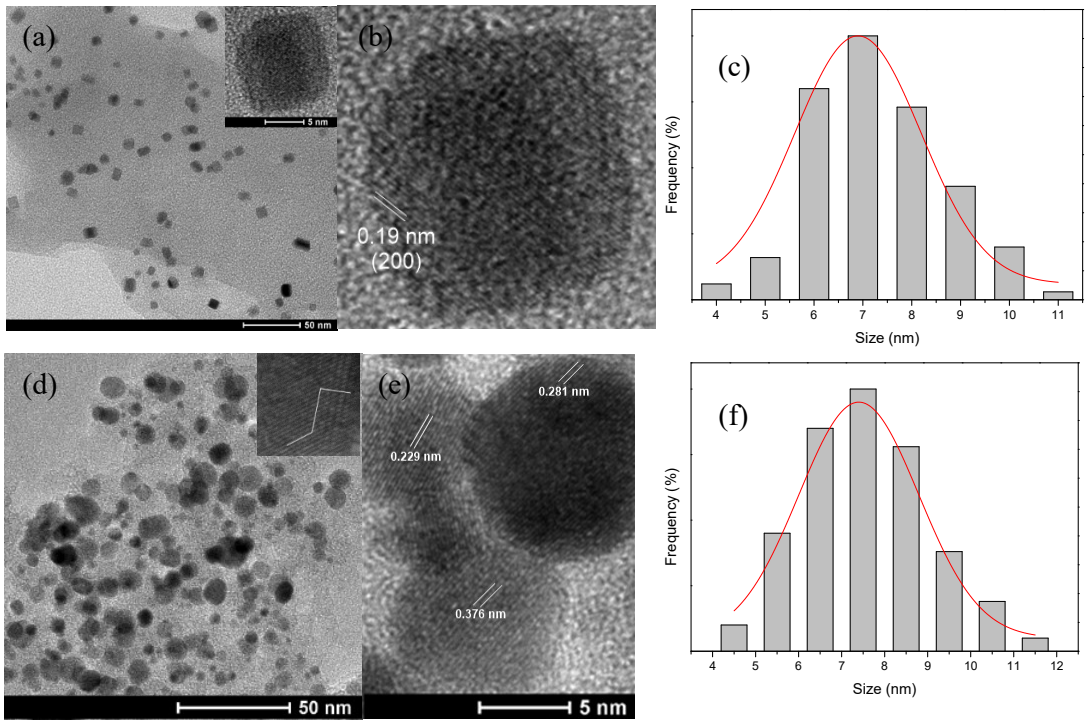

Fig. 1 (a) and (b) TEM and high-resolution TEM images of the as-synthesized **FePt-1** NPs; (c) size distribution of the NPs **FePt-1**; (d) and (e) TEM and high-resolution TEM images of **FePt-2**; (f) size distribution of the NPs **FePt-2**. The solid line represents the distribution which fitted the histogram.

In order to valid the above inference, the crystalline structures of the two types of NPs were identified by powder XRD analysis. The as-synthesized NPs **FePt-2** have chemically ordered fct phase FePt structures, evinced by the manifest (001) and (110) superlattice characterizing peaks. The average particle diameter is calculated to be 7.4 nm from the peak width of the XRD pattern using Scherer formula, which agrees with the TEM analysis. However, the XRD plot of **FePt-1** behaved different from the standard fct phase FePt, as shown in the red plot of **FePt-1** in Fig. 2, the (111) peak

moves left while the (200) peak moves to the right as compared to that for **FePt-2**. In addition, the (002) peak disappears in the plot for the **FePt-1**. So it can be inferred that the **FePt-1** are mostly in form of fct $FePt_3$ phase rather than FePt.[20, 35]

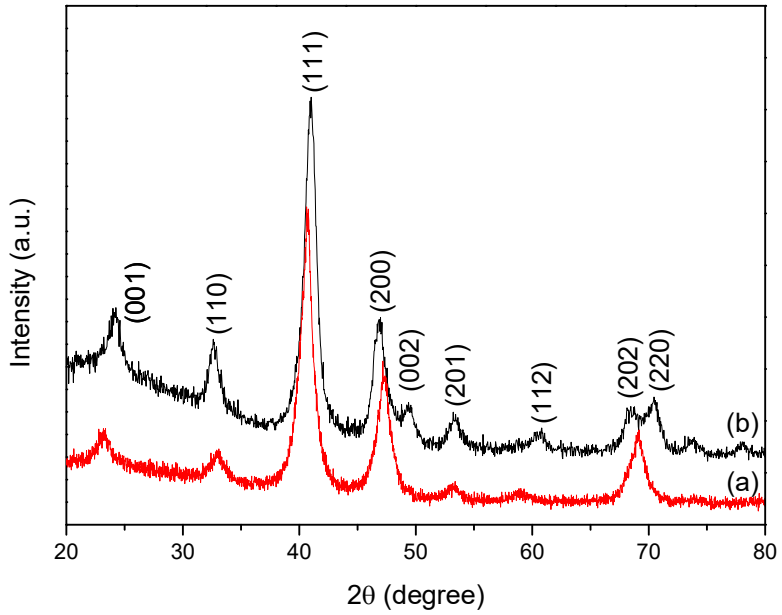

Fig. 2 Powder XRD pattern of FePt NPs (a) **FePt-1** and (b) **FePt-2** prepared from the single-source precursors of **TPy-FePt** and **P**, respectively.

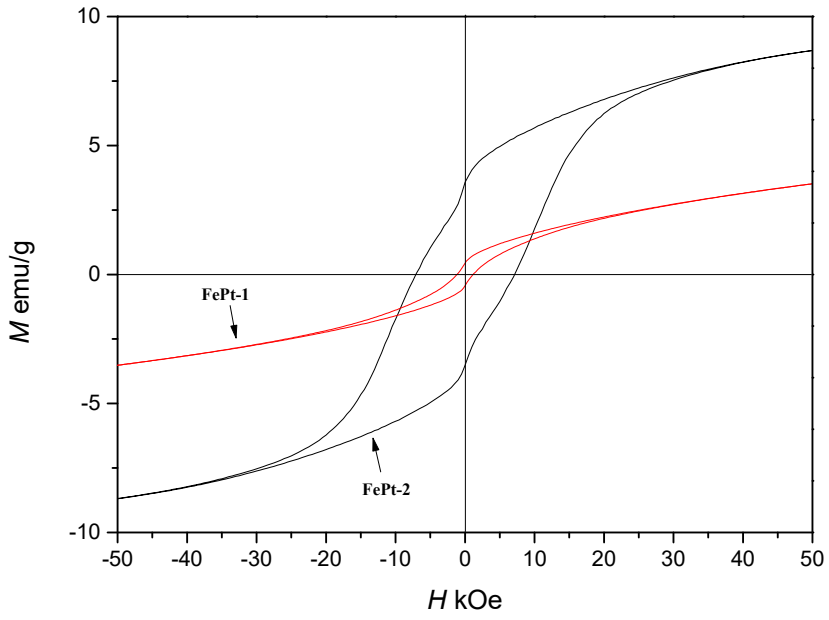

Fig. 3 Magnetic hysteresis loops of **FePt-1** and **FePt-2** at room temperature.

The magnetic properties of **FePt-1** and **FePt-2** were characterized by the magnetic hysteresis loops at room temperature with magnetic field up to 5T. Their coercivities were measured to be 0.6 kOe and 7.2 kOe, respectively. Higher magnetic moments per gram are observed in **FePt-2** as compared to that of **FePt-1**. Since the magnetic coercivity is higher for FePt over $FePt_3$, the magnetic properties results here further confirm that the **FePt-1** NPs as mostly $FePt_3$, while the **FePt-2** is FePt, which are consistent with the TEM and XRD results.

All the above results illustrated that the spatial structure of the NPs precursor has greatly effect on the nucleation processes of the FePt NPs. Influence by the metal-metal (Pt⋯Pt) and ligand π-π stacking interactions, Pt atoms have more chances to aggregate than Fe atoms.[36, 37] So the synthesized NPs from complex **TPy-FePt** are more likely to form Pt rich $FePt_3$ rather than FePt.[20] In contrast, the

metal atoms within the polymer skeleton **P** are randomly distributed with the covalent bond. So the Fe and Pt atoms have equal opportunity to combine during the pyrolysis, which leads to the resultant fct phase FePt NPs. In addition, the polymer chains might also play an important role in the formation of ordered FePt NPs.[38] As a result, $L1_0$ phase FePt NPs are easier to grow from metallic polymer **P** rather than the precursor **TPy-FePt**.

Patterning of ferromagnetic nanoline arrays

The fct phase FePt precursor metallopolymer **P** can be patterned on rigid substrate by direct NIL (Fig. 4). Using a PDMS mold with line patterns (750 nm periodicity and 350 nm feature size), inverse patterns of **P** are replicated on silicon substrate as shown in the SEM images Fig. 5a. The surface morphology of the nanoline patterned **P** was studied with AFM (Figure 5b), the height of the individual line was measured to be 70 nm.

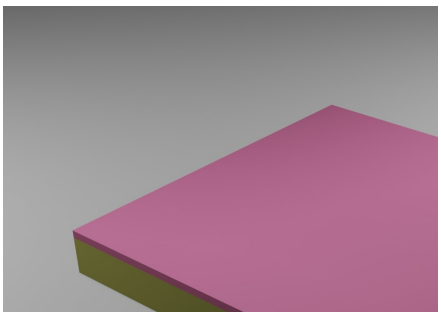

(a)

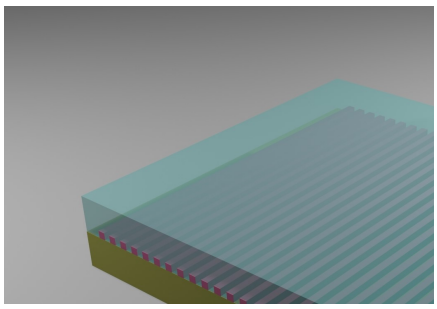

(b)

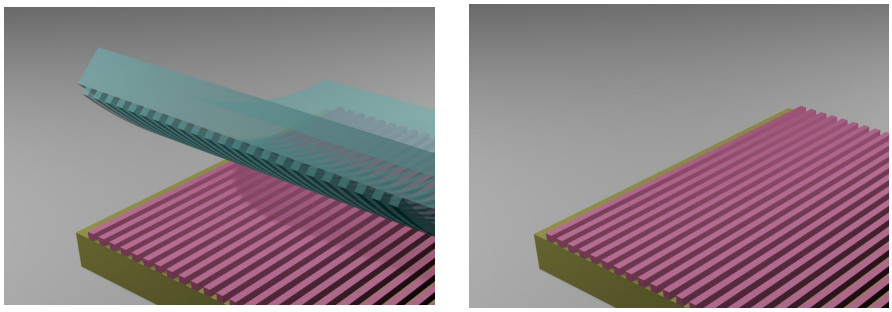

(c) (d)

Fig. 4 Schematic illustration of the NIL method. (a) Saturation solution of **P** was dipped onto a silicon substrate. (b) A stamped PDMS template with line arrays was imprinted immediately for 5 min under about 1 N gravity. (c) The template was removed and (d) the line patterning was left on the substrate, then it was pyrolyzed under Ar/H_2 for the preparation of FePt NPs.

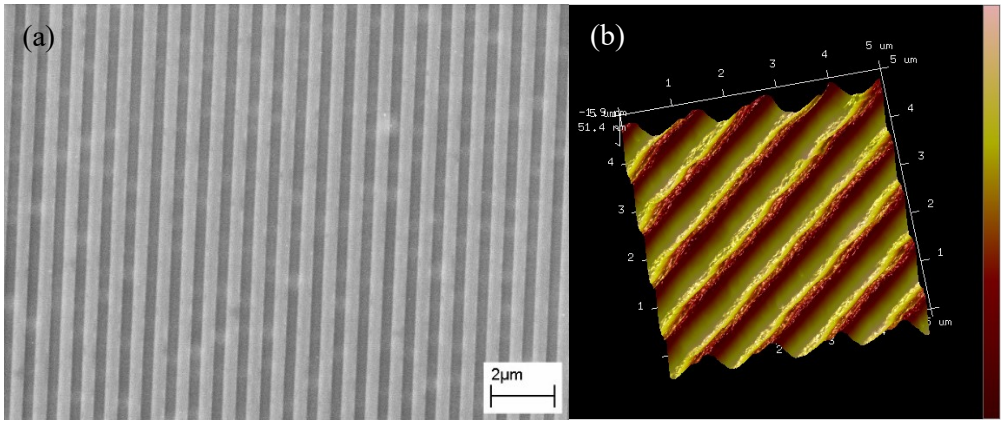

Fig. 5 FePt-embedded line arrays of polymer **P**: (a) SEM and (b) 3D AFM images.

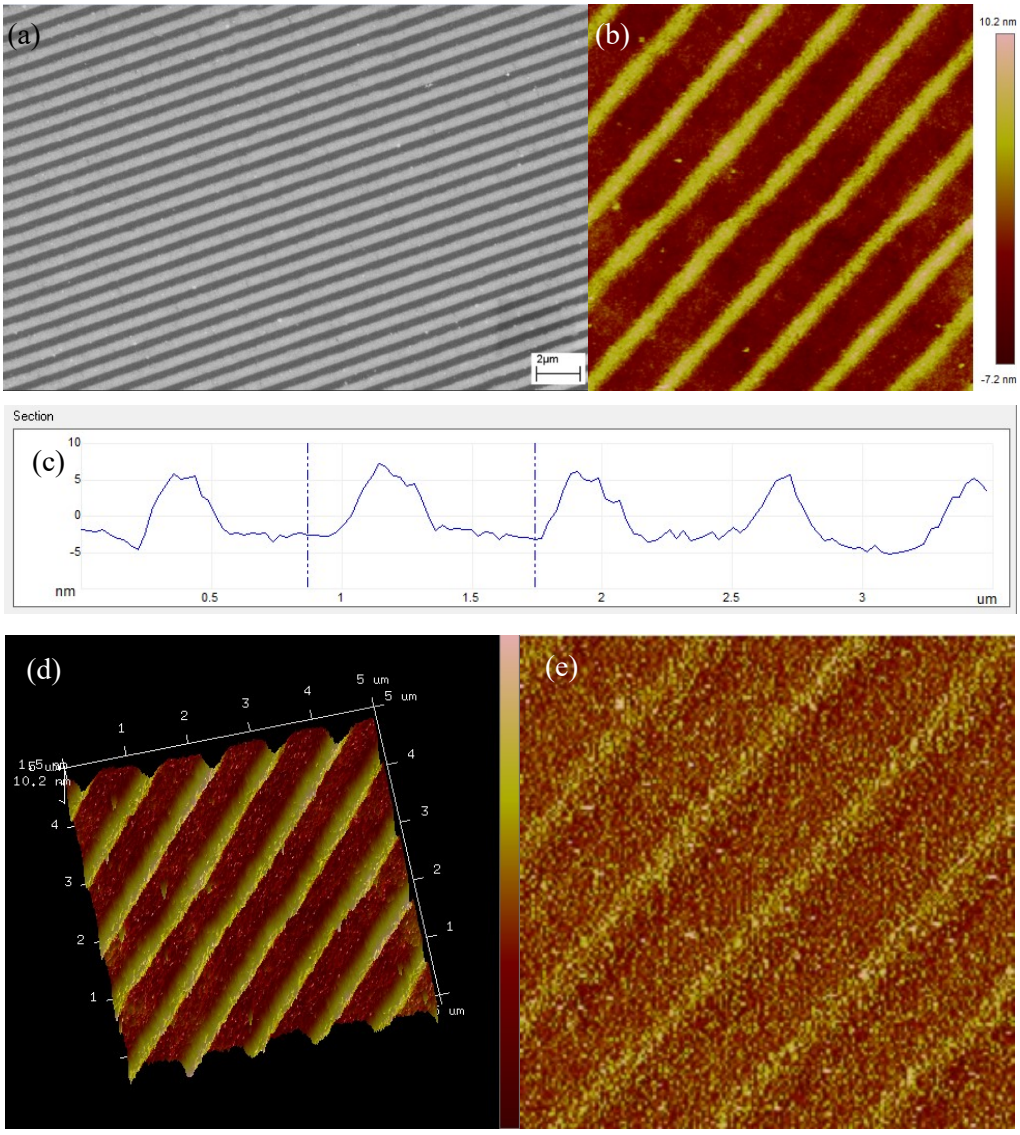

Fig. 6 Patterns with line arrays of FePt alloys after pyrolysis at 800 ºC under Ar/H_2: (a) SEM, (b) 2D AFM image, (c) cross-section measurement among the lines, (d) 3D AFM image and (e) MFM image.

After pyrolysis the patterned substrate, the featured nanoline structures were remained as shown in the SEM and AFM images in Figs. 6a and 6b, respectively. However, the height of the individual line is decreased to 10 nm revealed by the cross-section profile in Fig. 6c. The significant decrease of the height from 70 nm to 10 nm is

probably due to the carbon loss of **P** during pyrolysis process. Magnetic force microscopy (MFM) with interleave mode was also carried out to investigate the surface magnetic information of the **FePt-2** (Fig. 6e). Within the same area in Figure 5(e), the magnetic stray fields of the nanolines of FePt behave similar distributions. These nanolines made up of ferromagnetic FePt NPs with such obvious signals can work as rows of recording bits for bit patterned media.

Conclusions

Bimetallic compound **TPy-FePt** ([Pt(Fc-tpy)Cl]Cl) and its random copolymer **P** were synthesized and applied as single-source precursors for the preparation of FePt alloy NPs by direct pyrolysis. Phase transformation from FePt to $FePt_3$ was happened during the pyrolysis of **TPy-FePt**, and the resultant NPs have relatively poor magnetic coercivity. By introducing polymer skeleton, the resultant NPs **FePt-2** generated from **P** have a nearly equal atomic ratio of Fe to Pt and chemically ordered fct structure, which can be used as an effective single-source approach for the synthesis of $L1_0$ FePt NPs. It is thus expected that this type of metallopolymer can be applicable as a precursor for the fabrication of devices for magnetic recording media. Future work will be focusing on tuning the size of NPs by changing the molar fraction of individual blocks of metal and organic part in the metallopolymers which are compatible for bit patterned media fabricated by high throughout NIL.

Experimental

General

All the reactions were carried out under an atmosphere of nitrogen using standard Schlenk techniques as a matter of routine, although no special precautions were taken to exclude air or moisture during workup except the polymerization process. Solvents used in the polymer synthesis were dried and distilled from appropriate drying agents, then degassed before use. Styrene and trimethyl((4-vinylphenyl)ethynyl)silane were distilled from calcium hydride, azodiisobutylnitrile (AIBN) was recrystallized three times in EtOH before use. Other reagents were purchased and used as received.

All the reactions were monitored by thin-layer chromatography (TLC) with Merck pre-coated glass plates. Compounds were visualized with UV light irradiation at 254 and 365 nm. Purification of products was achieved by silica column chromatography. NMR spectra were measured in $CDCl_3$ or d_6-DMSO on a Bruker AV 400 NMR instrument with chemical shifts being referenced against tetramethylsilane as the internal standard for ^1H and ^{13}C NMR data. The molecular weight of the polymer was determined by Gel Permeation Chromatography (GPC) using a HP 1050 series HPLC instrument with visible wavelength and fluorescent detectors against polystyrene standards. IR spectra were recorded on the Nicolet Magna 550 Series II FTIR spectrometer using KBr pellets for solid state spectroscopy. Thermal analyses were performed with a Perkin-Elmer TGA 6 thermal analyzer.

The structural characterization of the as-synthesized FePt NPs was performed by PXRD on a Bruker AXS D8 Advance X-Ray Diffractometer, with Cu Kα (Running condition: 40 kV, 40 mA) for analyzing the composition and phase purity of the

resulting NPs, TEM on a Philips Tecnai G2 20 S-TWIN for probing the morphology, particle size and size distribution of NPs, EDX spectra on a LEO 1530 scanning electron microscope for studying the ratio of Fe and Pt in the resulting metal alloy NPs, X-ray photoelectron spectroscopy (XPS) on a SKL-12 spectrometer modified with VG CLAM 4 multichannel hemispherical analyzer for the detection of chemical composition of FePt NPs/C composite, and vibrating sample magnetometry (VSM) was applied for the magnetic hysteresis loops of FePt NPs.

Synthesis of TPy-FePt

4'-(Ferrocenyl)-[2,2':6',2'']terpyridine: The synthesis of 4'-(ferrocenyl)-[2,2':6',2'']terpyridine was reported by using the traditional two-steps synthetic route.[39] In this study, we optimized a new one-step reaction starting from readily available ferrocenylcaboxyaldehyde and 2-acetylpyridine to get the target compound. 2-Acetylpyridine (0.727 g, 6 mmol) was first added into a solution of ferrocenecarboxaldehyde (0.642 g, 3 mmol) in EtOH (40 mL). KOH pellets (0.455 g, 85%, 8.1 mmol) and aq. NH_3 (11.4 mL, 28%) were then added into the solution. The solution was stirred at 50 °C for 24 h. The mixture was then cooled to 20 °C, and the formed solid was collected by filtration and washed with ice-cold EtOH (10 mL). Recrystallization from EtOH afforded dark red crystalline solid (4.2 g, 13.0 mmol, 65%). ^{1}H NMR ($CDCl_3$, 400 Hz, δ/ppm) 8.75 (d, J = 4.7 Hz, 2H), 8.68 (d, J =7.9 Hz, 2H), 8.57 (s, 2H), 7.97 (td, J =7.8, 1.8 Hz, 2H), 7.46 (dd, J =6.9, 5.3 Hz, 2H), 5.12–4.90 (m, 2H), 4.59–4.41 (m, 2H), 4.11 (s, 5H). MALDI-TOF-MS: m/z calcd for

$C_{25}H_{19}FeN_3$: 417.09, found: 417.09 $[M]^+$.

TPy-FePt: Dimethyl sulfoxide (0.10 g, 1.5 mmol) was added into a solution of K_2PtCl_4 (0.21 g, 0.5 mmol) in water (10 mL), and the mixture was left at ambient temperature for 3 h. The yellow solid was then collected by filtration, washed with water, followed by ethanol and diethyl ether, and dried in vacuo to give $[(DMSO)_2Pt(Cl)_2]$ (0.18 g, 0.4 mmol, 89%).

A mixture of 4'-(ferrocenyl)-[2,2':6',2'']terpyridine (41.7 mg, 0.1 mmol) and $(DMSO)_2PtCl_2$ (42.2 mg, 0.1 mmol) in $CHCl_3$ (50 mL) was stirred and refluxed overnight. After cooling to room temperature, the product was filtered off and washed with water. Subsequent recrystallization by diffusion of diethyl ether vapor into a solution of the product in acetonitrile gave pure **TPy-FePt** (58 mg, 90 %) as green solid. ^{1}H NMR (*d*$_6$-DMSO, 400 MHz, δ/ppm) 8.90 (d, *J* = 5.6 Hz, 2H), 8.77 (d, *J* = 8.0 Hz, 2H), 8.59 (s, 2H), 8.52 (t, *J* = 7.8 Hz, 2H), 7.98–7.87 (m, 2H), 5.41 (s, 2H), 4.82 (s, 2H), 4.21 (s, 5H). MALDI-TOF-MS: m/z calcd for $[C_{25}H_{19}ClFeN_3Pt]^+$: 647.03, found: 647.24 $[M]^+$.

Synthesis of copolymer P

Trimethyl((4-vinylphenyl)ethynyl)silane (TMSES): To an ice-cooled mixture of 4-bromostyrene (1.4 mg, 7.6 mmol) in freshly distilled triethylamine (25 ml) and dichloromethane (25 ml) solution, CuI (50 mg), $Pd(OAc)_2$ (50 mg) and PPh_3 (150 mg) were added. After the solution was stirred for 30 min at 0 °C, trimethylsilylacetylene (5 ml, 38 mmol) was then introduced and the suspension was stirred for 30 min in an

ice-bath before being warmed to room temperature. After reacting for 30 min at room temperature, the mixture was heated to 75 °C for 24 h. The solution was then allowed to cool at room temperature and the solvent mixture was evaporated in vacuo. The crude product was purified by column chromatography on silica gel with *n*-hexane as eluent to generate **TMSES** as an oil (1.23 g, 81%). ^{1}H NMR ($CDCl_3$, 400 MHz, δ/ppm): 7.42 (d, *J* = 7.9 Hz, 2H, Ar-H), 7.34 (d, *J* = 8.2 Hz, 2H, Ar-H), 6.72–6.65 (m, 1H, vinyl-H), 5.76 (dd, *J* = 17.6, 0.7 Hz, 1H, vinyl-H), 5.29 (dd, *J* = 10.9, 0.6 Hz, 1H, vinyl-H), 0.26 (s, 9H, -Si(CH_3)$_3$); ^{13}C NMR ($CDCl_3$, 100 MHz, δ/ppm): 137.6, 136.2, 132.1, 126.0, 122.4, 114.8, 105.1, 94.8, 0.3.

PTMSES-PS: This block copolymer was synthesized by free radical polymerization. In this reaction, styrene (2.04 g, 19.6 mmol), **TMSES** (81.4 mg, 0.4 mmol) and AIBN (114 mg, 5 mol%) in 5 mL of THF were combined in a 25 mL Schlenk tube and degassed by subjecting the mixture to three freeze-dry-thaw cycles under nitrogen. The mixture was heated under 80 ºC for 15 hr and then cooled to room temperature. The resulting polymer was dissolved in a minimum of THF, precipitated in methanol (100 mL), centrifuged to separate. After precipitating three times by using a THF-methanol system, the white solid was dried under high vacuum to obtain the targeted product, the ratio of blocks was found to be 47:1 PS:PTMSES by ^{1}H NMR. ^{1}H NMR ($CDCl_3$, 400 MHz, δ/ppm) 7.5–6.25 (m, Ar-H), 2.00–0.80 (m, PTMSES backbone), 0.28 (s, Si(CH_3)$_3$). IR (KBr, cm^{-1}) 2109 (C≡C). M_n = 9830, M_w = 15546, PDI = 1.58.

PES-PS: The deprotection of TMS in polymer was carried out by the modified

literature.[40] The polymer **PTMSES-PS** (2.380 g) was dissolved in dry THF (10 mL), and the solution was cooled at 0 ºC. $(C_4H_9)_4NF$ in THF (1 M, 2 mL) was added to the solution, and the mixture was stirred at 0 ºC for 1 h. The polymer was precipitated in methanol and purified twice by precipitation using a THF-methanol system. The yield of polymer was quantitative. ^{1}H NMR ($CDCl_3$, 400 MHz, δ/ppm) 7.5–6.25 (m, Ar–H), 3.75 (s, C≡CH), 2.00–0.80 (m, TMSES backbone). IR (KBr, cm^{-1}) 2109 (C≡C), 3294 (C≡C–H).

P: A mixture of **PES-PS** (0.5 g) and **TPy-FePt** (71 mg) was dissolved in NEt_3/DMF (20 mL, 1:1 v/v), followed by the addition of CuI (2 mg). The solution was stirred overnight under a nitrogen atmosphere at room temperature. Dark-green precipitate was obtained by filtration and washed with diethyl ether. Subsequent recrystallization by diffusion of diethyl ether vapor into a solution of the product in acetonitrile gave **P** in quantitative yield as black solid. ^{1}H NMR ($CDCl_3$, 400 MHz, δ/ppm) 8.90–8.52 (m, Py-H), 7.98–7.87 (m, Ar-H), 5.41–4.21 (m, Fc–H), 7.52–6.25 (m, Ar–H), 2.00–0.80 (m, PTMSES backbone). IR (KBr, cm^{-1}): 2109 (C≡C). T_{onset} = 291 ºC.

Preparation of FePt NPs

The $L1_0$ FePt alloy **FePt-2** NPs was prepared by direct pyrolysis under Ar/H_2 (5 wt%) atomosphere. The metallopolymer **P** was placed in a ceramic boat inside a quartz tube in a furnace. The tube was purged with Ar/H_2 atmosphere and heated to the desired temperature 500 ºC at a rate of 10 ºC/min and held for 1 h. After cooling

to room temperature, the tube were then heated to 800 ºC and held for 1 h, **FePt-2** was formed. **FePt-1** NPs was synthesized similarly by the pyrolysis of complex **TPy-FePt**.

Fabrication of magnetic nanoline patterning from the polymer P

Saturation solution of **P** was prepared in $CHCl_3$. After filtered with 0.22 μm hydrophobic syringe filters, a small amount of the solution was dipped onto a silicon substrate and a stamped PDMS template with line arrays was imprinted immediately for 5 min under about 1 N gravity. The template was removed and the line patterning was left on the substrate, then it was pyrolyzed under Ar/H_2 according to the same conditions as the preparation of FePt NPs. The resulting ferromagnetic line arrays was then characterized by SEM, AFM and MFM.

Acknowledgments

Z. Meng and G. Li contributed equally to this work. C.-L. Ho thanks Hong Kong Baptist University (FRG2/13-14/078) and the Science, Technology and Innovation Committee of Shenzhen Municipality (JCYJ20140818163041143) for their financial support.

References

1. W. J. Liu, T. T. Qian and H. Jiang, *Chem. Eng. J.*, 2014, **236**, 448–463.

2. H. L. Jiang, T. Akita, T. Ishida, M. Haruta and Q. Xu, *J. Am. Chem. Soc.*, 2011,

133, 1304−1306.

3. X. H. Peng, Q. M. Pan and G. L. Rempel, *Chem. Soc. Rev.*, 2008, **37**, 1619−1628.

4. W. H. Chiang and R. M. Sankaran, *Adv. Mater.*, 2008, **20**, 4857−4861.

5. A. Ethirajan, U. Wiedwald, H. G. Boyen, B. Kern, L. Y. Han, A. Klimmer, F. Weigl, G. Kastle, P. Ziemann, K. Fauth, J. Cai, R. J. Behm, A. Romanyuk, P. Oelhafen, P. Walther, J. Biskupek and U. Kaiser, *Adv. Mater.*, 2007, **19**, 406−410.

6. B. D. Terris and T. Thomson, *J. Phys. D. Appl. Phys.*, 2005, **38**, R199−R222.

7. D. Weller, S. H. Sun, C. Murray, L. Folks and A. Moser, *IEEE Trans. Magn.*, 2001, **37**, 2185−2187.

8. Q. Li, L. H. Wu, G. Wu, D. Su, H. F. Lv, S. Zhang, W. L. Zhu, A. Casimir, H. Y. Zhu, A. Mendoza-Garcia and S. H. Sun, *Nano Lett.*, 2015, **15**, 2468−2473.

9. S. J. Guo and S. H. Sun, *J. Am. Chem. Soc.*, 2012, **134**, 2492−2495.

10. T. Burkert, O. Eriksson, S. I. Simak, A. V. Ruban, B. Sanyal, L. Nordstrom and J. M. Wills, *Phys. Rev. B*, 2005, **71**, 134411.

11 S. H. Sun, C. B. Murray, D. Weller, L. Folks and A. Moser, *Science*, 2000, **287**, 1989−1992.

12 K. E. Elkins, T. S. Vedantam, J. P. Liu, H. Zeng, S. H. Sun, Y. Ding and Z. L. Wang, *Nano Lett.*, 2003, **3**, 1647−1649.

13 R. Harpeness and A. Gedanken, *J. Mater. Chem.*, 2005, **15**, 698−702.

14 C. Liu, X. W. Wu, T. Klemmer, N. Shukla, X. M. Yang, D. Weller, A. G. Roy,

M. Tanase and D. Laughlin, *J. Phys. Chem. B*, 2004, **108**, 6121–6123.

15. H. Sun, *Adv. Mater.*, 2006, **18**, 393–403.

16. T. Hyeon, *Chem. Commun.*, 2003, 927–934.

17. S. Kang, J. W. Harrell and D. E. Nikles, *Nano Lett.*, 2002, **2**, 1033–1036.

18. S. Saita and S. Maenosono, *Chem. Mater.*, 2005, **17**, 3705–3710.

19. J. C. Bauer, X. Chen, Q. S. Liu, T. H. Phan and R. E. Schaak, *J. Mater. Chem.*, 2008, **18**, 275–282.

20. H. M. Song, W. S. Kim, Y. B. Lee, J. H. Hong, H. G. Lee and N. H. Hur, *J. Mater. Chem.*, 2009, **19**, 3677–3681.

21. H. M. Song, J. H. Hong, Y. B. Lee, W. S. Kim, Y. Kim, S. J. Kim and N. H. Hur, *Chem. Commun.*, 2006, 1292–1294.

22. M. S. Wellons, W. H. Morris, Z. Gai, J. Shen, J. Bentley, J. E. Wittig and C. M. Lukehart, *Chem. Mater.*, 2007, **19**, 2483–2488.

23. A. Capobianchi, M. Colapietro, D. Fiorani, S. Foglia, P. Imperatori, S. Laureti and E. Palange, *Chem. Mater.*, 2009, **21**, 2007–2009.

24. Q. Dong, G. J. Li, H. Wang, P. W. T. Pong, C. W. Leung, I. Manners, C.-L. Ho, H. Li and W.-Y. Wong, *J. Mater. Chem. C*, 2015, **3**, 734–741.

25. Q. Dong, G. J. Li, C.-L. Ho, M. Faisal, C. W. Leung, P. W. T. Pong, K. Liu, B. Z. Tang, I. Manners and W. -Y. Wong, *Adv. Mater.*, 2012, **24**, 1034–1040.

26. K. Liu, C.-L. Ho, S. Aouba, Y. Q. Zhao, Z. H. Lu, S. Petrov, N. Coombs, P. Dube, H. E. Ruda, W.-Y. Wong and I. Manners, *Angew. Chem. Int. Ed.*, 2008, **47**, 1255–1259.

27. G. J. Li, C. W. Leung, Z. Q. Lei, K. W. Lin, P. T. Lai and P. W. T. Pong, *Thin Solid Films*, 2011, **519**, 8307–8311.

28. S. Y. Chou, P. R. Krauss and P. J. Renstrom, *Appl. Phys. Lett.*, 1995, **67**, 3114–3116.

29. H. Schift, *J. Vac. Sci. Technol. B*, 2008, **26**, 458–480.

30. S. Y. Chou, P. R. Krauss, W. Zhang, L. J. Guo and L. Zhuang, *J. Vac. Sci. Technol. B*, 1997, **15**, 2897–2904.

31. D. Morecroft, J. K. W. Yang, S. Schuster, K. K. Berggren, Q. F. Xia, W. Wu and R. S. Williams, *J. Vac. Sci. Technol. B*, 2009, **27**, 2837–2840.

32. Q. C. Dong, G. J. Li, C.-L. Ho, C. W. Leung, P. W. T. Pong, I. Manners and W.-Y. Wong, *Adv. Funct. Mater.*, 2014, **24**, 857–862.

33. B. Tang, F. Yu, P. Li, L. L. Tong, X. Duan, T. Xie and X. Wang, *J. Am. Chem. Soc.*, 2009, **131**, 3016–3023.

34. O. Margeat, M. Tran, M. Spasova and M. Farle, *Phys. Rev. B*, 2007, **75**, 134410.

35. Y. Liu, Y. H. Jiang, X. L. Zhang, Y. X. Wang, Y. J. Zhang, H. L. Liu, H. J. Zhai, Y. Q. Liu, J. H. Yang and Y. S. Yan, *J. Solid State Chem.*, 2014, **209**, 69–73.

36. L. B. Xing, S. Yu, X. J. Wang, G. X. Wang, B. Chen, L. P. Zhang, C. H. Tung and L. Z. Wu, *Chem. Commun.*, 2012, **48**, 10886–10888.

37. K. Mitra, U. Basu, I. Khan, B. Maity, P. Kondaiah and A. R. Chakravarty, *Dalton Trans.*, 2014, **43**, 751–763.

38. E. Kang, H. Jung, J. G. Park, S. Kwon, J. Shim, H. Sai, U. Wiesner, J. K. Kim

and J. Lee, *ACS nano*, 2011, **5**, 1018−1025.

39. E. C. Constable, A. J. Edwards, R. Martinezmanez, P. R. Raithby and A. M. W. C. Thompson, *J. Chem. Soc. Dalton*, 1994, 645−650.

40. K. Tsuda, T. Ishizone, A. Hirao and S. Nakahama, *Macromolecules*, 1993, **26**, 6985−6991.